Applied Physics A (2019) 125:1
https://doi.org/10.1007/s00339-018-2286-x

Applied Physics A
Materials Science & Processing

Erbium-doped chalcogenide glass thin film on silicon using femtosecond pulsed laser with different deposition temperatures

K. S. Albarkaty[1] · E. Kumi-Barimah[1] · C. Craig[2] · D. Hewak[2] · G. Jose[1] · J. Chandrappan[1]

Received: 5 September 2018 / Accepted: 27 November 2018
© The Author(s) 2018

Abstract
The properties of Er^{3+}-doped gallium lanthanum sulphide thin films prepared on a silicon substrate by femtosecond pulsed laser deposition were studied as a function of process temperature. The films were characterised using transition electron microscopy imaging, X-ray diffractometry, Raman spectroscopy, fluorescence spectroscopy, and UV–Vis–NIR spectroscopy. The results show that by increasing the substrate temperature, the deposited layer thickness increases and the crystallinity of the films changes. The room temperature photoluminescence and lifetimes of the $^4I_{13/2}\rightarrow{}^4I_{15/2}$ transition of Er^{3+} are reported in the paper.

1 Introduction

Chalcogenide glasses consist of chalcogen elements such as sulphur, selenium, and tellurium from the Group VI of the periodic table, and then mixed with other additive elements such as germanium (Ge), arsenic (As), antimony (Sb), and gallium (Ga) [1, 2]. These glasses have numerous applications in the near-infrared (NIR) and mid-infrared (MIR), especially the high transparency window from 1 to 10 µm make them ideal for passive optical device applications [3–6]. When incorporated with rare earth ions such as ytterbium (Yb), erbium (Er), neodymium (Nd), thulium (Tm), praseodymium (Pr), and holmium (Ho), they offer additional applications in long-wavelength light-emitting and amplification devices [2–4]. Furthermore, an extension of these materials study into the MIR wavelength would be suitable for active optical devices (e.g. IR fibre-optic amplifiers operating in the 2–10 µm range) and a wide range of spectroscopy (e.g. diffuse reflectance and absorption) and sensing (e.g. fibre-optic chemical sensor systems) of applications [7–9]. These applications benefit integration of chalcogenide glass-based active and passive components into a single substrate, which would eventually reduce the device footprint and cost [10]. For instance, Ga–La–S glass has been known and studied extensively for many years as an alternative glass to toxic As and Ge-chalcogenide-based compounds. An inherent low phonon energy makes them attractive for rare earth doping for reducing the rate of non-radiative recombination and enhancing the radiative efficiency of the rare earth ions emissions [11–13]. These glasses also support high doping concentration of the rare earth ions, leading to high refractive index ($n = 2.4$–3.0) and low-loss transmission glasses for photonic device engineering. Ye et al. [13] have demonstrated high fluorescence efficiency of Er-doped Ga–La–S glass at 1.54 µm, which has clear advantages over silica glasses for manufacturing optical waveguide amplifiers utilising $^4I_{13/2} \rightarrow {}^4I_{15/2}$ transition. Frantz et al. [14] reported Er-doped Ga–La–S glass thin film on silica substrate for waveguide amplifiers operating at a wavelength of 1.5 µm, and a maximum optical gain of 2.8 dB/cm at 1.5 µm of the Er^{3+} ion transition was obtained. Furthermore, the laser action of Nd-doped Ga–La–S glass pulled into fibres with core/clad structures has been demonstrated by Schweizer et al. [15].

Various fabrication methods have been utilised to prepare rare earth ions doped/or undoped chalcogenide thin film, including chemical vapour deposition (CVD) [16, 17], spin coating [18–20], magnetron sputtering [15, 21, 22] and pulsed laser deposition (PLD) [23–26]. For example, sputtering produces films with an acceptable stoichiometric composition identical to the target material. The PLD technique has many similarities to the sputtering method and is considered as one of the most promising techniques

✉ E. Kumi-Barimah
preeku@leeds.ac.uk

[1] School of Chemical and Process Engineering, University of Leeds, Leeds LS2 9JT, UK

[2] The Optoelectronics Research Centre, University of Southampton, Southampton SO17 1BJ, UK

Published online: 05 December 2018

capable of producing uniform thin films or multilayer structures without changing the stoichiometric composition. It is also a highly flexible system, which consists of a wide range of deposition parameters making possible to synthesise a large variety of thin films of complex chemical composition and can provide higher doping concentrations without major fluorescence and lifetime quenching. Recently, picosecond (ps) to femtosecond (fs) regimes (short and ultrashort pulse durations) PLD have been employed to fabricate thin films, and then for material processing due to their unique advantages over the conventional PLD nanosecond (ns) and microsecond (ms) pulsed lasers (long pulse durations) [27, 28]. For instance, ablation mechanism of short and ultrashort pulse PLD is quite different from long pulse lasers, because they have ablation rate of about 30–40 times higher than those of ns and ms PLDs [29]. On the other hand, the ns and ms pulse lasers such as excimer and YAG lasers induce damage through heating and melting processes, and ablation process and thermal decomposition generate considerable high-temperature gradient or heat-affected zone in bulk material with a laser-induced shock [30]. This does not provide the needed thin film quality in complex materials, as the particle size generated becomes broader and clustered. Short and ultrashort laser regime ablation leads to minimum heat-affected zone and without collateral damage to the target surface [28]. When the short and ultrashort lasers' energy interacts with the target material, their energies are absorbed by free electrons on the target surface, which consists of partially ionised vapour and a plume of hot nanoparticles via fragmentation and phase explosion, and homogeneous nucleation and decomposition [30, 31].

In this paper, we employ fs-PLD to deposit high-quality Er^{3+} -doped Ga–La–S glass thin films on a silicon substrate. The structure and optical properties of as-deposited thin films under three different temperatures are reported for possible optical waveguide applications in the NIR.

2 Experimental setup

In this study, Ti:sapphire fs laser (wavelength = 800 nm, pulse repetition rate = 1 kHz, and pulse duration = 100 fs) shown in Fig. 1 has been employed to deposit Er^{3+} ion-doped Ga–La–S thin film on a silicon substrate at various temperatures. The Er^{3+}-doped Ga–La–S glass target has a composition of Ga–La–S 65:34 + 1 mol % Er_2O_3 ingot from ChG Southampton Ltd. Initially, the target and the commercially available silicon substrate of dimensions 20 mm (L) × 12 mm (W) × 675 μm (T) were mounted in their respective holders inside the chamber. Both target and substrate holders were allowed to rotate continuously at a constant speed of 40 rpm and 20 rpm, respectively, while the target-to-substance distance was kept at 70 mm. The vacuum chamber waspumped down to about 10^{-5} Torr to remove any water residues in the chamber and then filled at a low flow rate of 20 sccm argon (Ar) to maintain 80

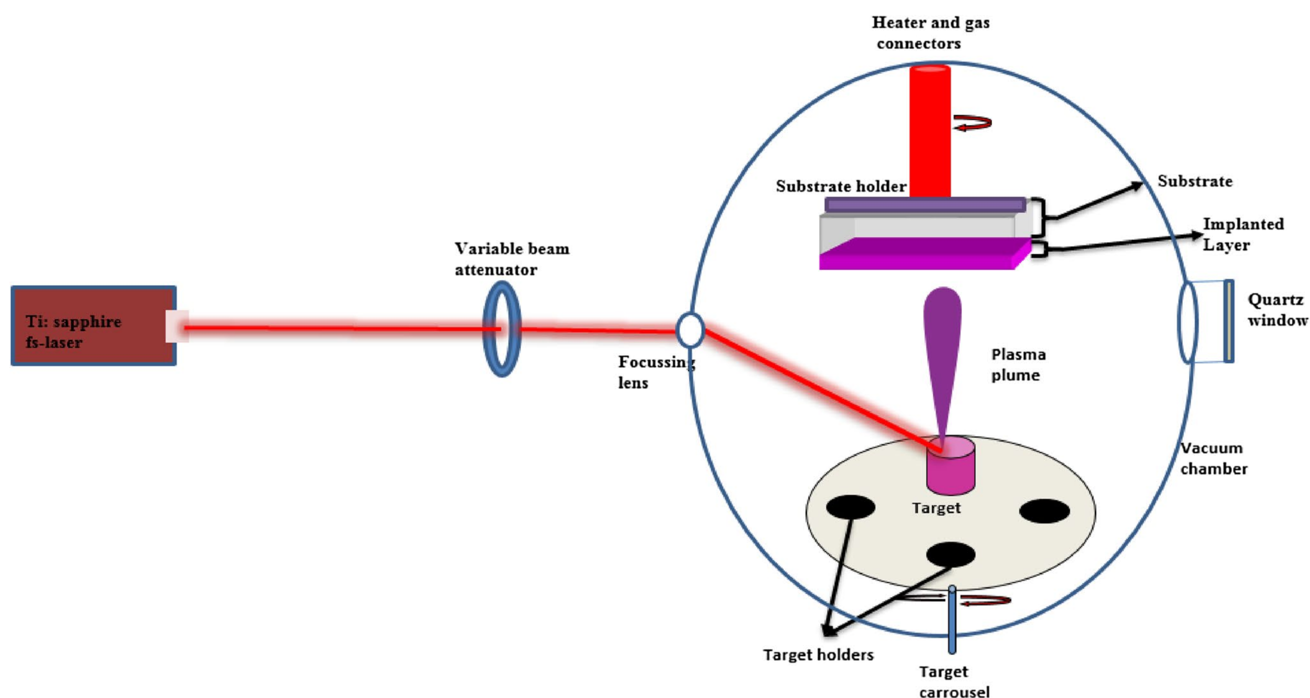

Fig. 1 Schematic setup of the fs-pulsed laser deposition system (PLD)

mTorr throughout the process. The fs laser of pulse energy 50 μJ was focused onto the target material at an angle of 60° to generate plasma plume directed perpendicular to the substrate surface. Three samples, GE1, GE2, and GE3, were prepared at temperatures of 25 °C, 450 °C and 660 °C, respectively, for 4 h. The processed sample was kept in the vacuum chamber under the argon atmosphere and naturally cooled to room temperature.

The surface morphology and thin film thickness were obtained using an FEI Titan Themis Cubed 300 transmission electron microscopy (TEM) and high-resolution monochromated field emission gun scanning electron microscope (FEGSEM) with a precise focused ion beam (FIB) (FEI Helios G4 CX DualBeam). To investigate and understand the structural characteristics of the deposited film, Raman spectroscopy and X-ray diffraction (XRD) were utilised. A Renishaw inVia Raman spectrometer was employed to measure the Raman scattering spectra with an Ar^+ laser (514 nm) excitation source. Furthermore, the XRD patterns of the target sample and films were determined using a Philips X'Pert with Cu Kα radiation ($\lambda = 1.54056$ Å), at 40 kV and 100 mA. Each sample was scanned for 60 min with a diffractometer angle range from 10° to 60° in a step size of 0.033°. NIR emission spectra and lifetime of the Er^{3+}-doped Ga–La–S bulk sample and as-deposited thin films were measured using a fluorescence spectrometer (FS920; Edinburgh Instruments, UK) equipped with semiconductor laser diode emitting 980 nm excitation source at room temperature. The transmission property of the thin films was measured by PerkinElmer Lambda 950 High-Performance UV–Vis/NIR Spectrometers to estimate the optical band gap.

3 Results and discussion

3.1 The structural characteristics of the Er^{3+}-doped Ga–La–S thin films

Figure 2a–c illustrates the TEM cross-sectional images of the films processed using an Er^{3+}-doped Ga–La–S target at different substrate temperatures while keeping other process parameters constant. The plan view of TEM measurements reveals an average film thickness around 45 nm, 95 nm, and 208 nm for samples GE1, GE2, and GE3, respectively. It can be noted that an increase in deposition substrate temperature has a significant effect on the film thickness. Figure 2d shows the cross-sectional elemental mapping images obtained for GE3, which confirmed that the deposited layer consisted of the uniform distribution of the Ga, La, S, and Er elements. However, there is no intermixing between the Er^{3+}-doped Ga–La–S coating and the silicon substrate network observed in the interface.

Further quantification of a silicon substrate, a bulk glass and a thin film of the Er-doped Ga–La–S surface morphology with XRD pattern is illustrated in Fig. 3. As seen in Fig. 3, the silicon substrate exhibits two main sharp peaks centred at 36.24° and 55.62°, which validates the crystallinity of the substrate. The more intense peak centred at 55.62° is in good agreement with an ICDD (International Centre for Diffraction Data) pattern No. 00-005-0565 for silicon (not shown here), while the other peak that occurs at 36.24° correlated with the ICDD diffraction pattern No. 00-039-1425 corresponds to silica. On the other hand, no peak is observed from the bulk target glass; however, XRD data reveals a wide-stretched halo amorphous structure between $2\theta = 20°$ and 30°.

Conversely, the XRD pattern of the Er^{3+}-doped Ga–La–S thin film deposited at room temperature (GE1) did not possess any additional peaks compared to the silicon substrate. This clearly confirms the amorphous property of the film and further evidence is provided with discussion of Raman spectra reported in Fig. 4. However, sample GE2 prepared at higher temperature displayed two crystalline peaks centred at $2\theta = 25°$ and 28°, which are not found in sample GE1. Furthermore, when the substrate temperature is increased to 660 °C (GE3), it reveals similar crystalline peaks observed in sample GE2 and three new crystalline peaks at $2\theta = 25°$, 45°, and 47°. Comparing the XRD patterns of samples GE2 and GE3 on HighScore database, these crystalline phase peaks observed are in agreement with $La_6Ga_{3.3}S_{14}$, $La_3Ga_{1.67}S_7$, and $LaGaS_3$ which correlate with diffraction patterns No. 00-01-081-5771, 00-04-005-8197, and 00-04-017-0337. A similar observation had been reported previously by Frantz et al. [14], where the author concluded that such crystal phase's formation can be attributed to quenching and/or heat treatment of the Ga–La–S target glass. Additionally, the crystallite size was calculated from the XRD data for peaks occurring around $2\theta = 25°$ and 29° through Debye–Scherer formula [32]:

$$D_{(hkl)} = \frac{K}{\beta \cdot \cos\theta},$$

where λ is the X-ray wavelength (0.15405 nm), β is the full width at half width at full maximum of the diffraction peak, and K is a constant related to crystallite shape (0.9). The average crystallite size for samples GE2 (450 °C) and GE3 (660 °C) was calculated to be ~5 nm and 15 nm, respectively. This shows that the crystallite size increases from 5 to 15 nm with increasing deposition temperature from 450 to 660 °C.

Figure 4 represents the Raman spectra for a pure silicon substrate, a bulk target, and thin films prepared at various temperatures when excited by a 514.5 nm argon laser. The silicon substrate spectrum exhibits a sharp

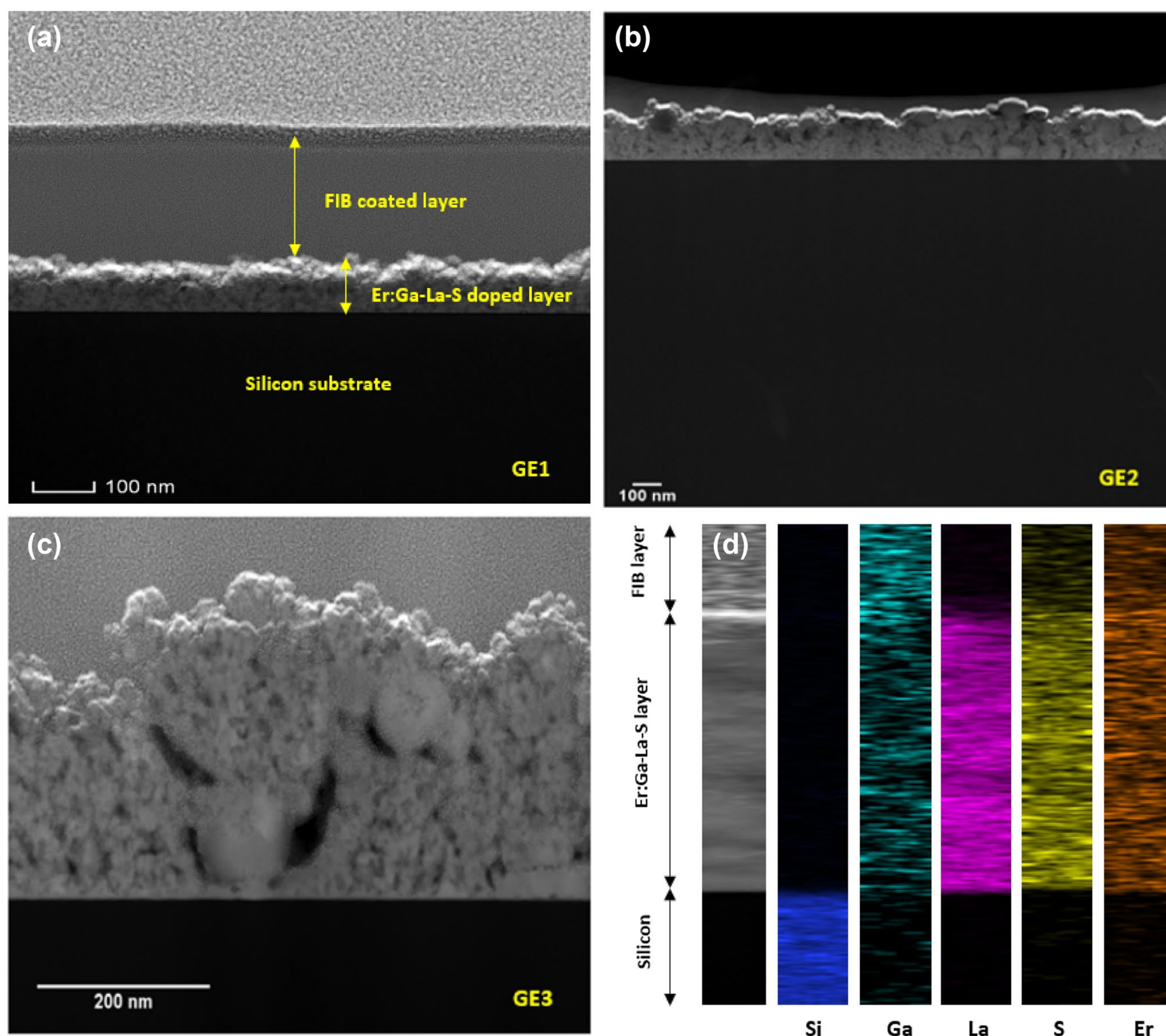

Fig. 2 **a**–**c** TEM cross-sectional images of Er^{3+}-doped Ga–La–S thin films deposited at different substrate temperatures: **a** 25 °C, **b** 450 °C, and **c** 660 °C. **d** Energy-dispersive X-ray spectroscopy (EDX) elemental mapping obtained during cross-sectional TEM analysis of a GE3 sample prepared at 660 °C

peak with a characteristic band at 520 cm^{-1}, attributed to single crystalline silicon. Furthermore, the Raman spectrum of Er^{3+}-doped bulk Ga–La–S glass consists of three main group bands at 190–920 cm^{-1}, 920–1200 cm^{-1}, and 1200–1800 cm^{-1}. The broad band centred around 420 cm^{-1} corresponds to GaS_4 tetrahedron stretching vibration modes or vibration of LaS_8 structural [26] units present in amorphous Ga–La–S. The broad bands at higher frequencies (centred at 1200 cm^{-1} and 1300 cm^{-1}, respectively) are from Er^{3+} photoluminescence (PL) corresponding to $^2H_{11/2}$–$^4I_{15/2}$ (547 nm) and $^4S_{3/2}$–$^4I_{15/2}$ (553 nm) transitions in a glassy medium [33, 34].

In addition to this, Raman spectra of all the thin film samples prepared by the fs-PLD were also investigated. The sample prepared at 25 °C (GE1) reveals no assigned Raman bands of the Er^{3+}-doped Ga–La–S glass, but only a single crystalline peak in the Raman spectrum of the silicon substrate. By increasing deposition temperature of the substrate to 450 °C (GE2) and 660 °C (GE3), the Raman spectra reveal five bands with the maximum peak intensities centred around 335 cm^{-1}, 495 cm^{-1}, 644 cm^{-1}, 1200 cm^{-1}, and 1350 cm^{-1}. The Raman sharper bands peaking at 335 cm^{-1}, 495 cm^{-1}, and 644 cm^{-1} are correlated to the vibrations of LaS_8 or GaS_4 tetrahedron

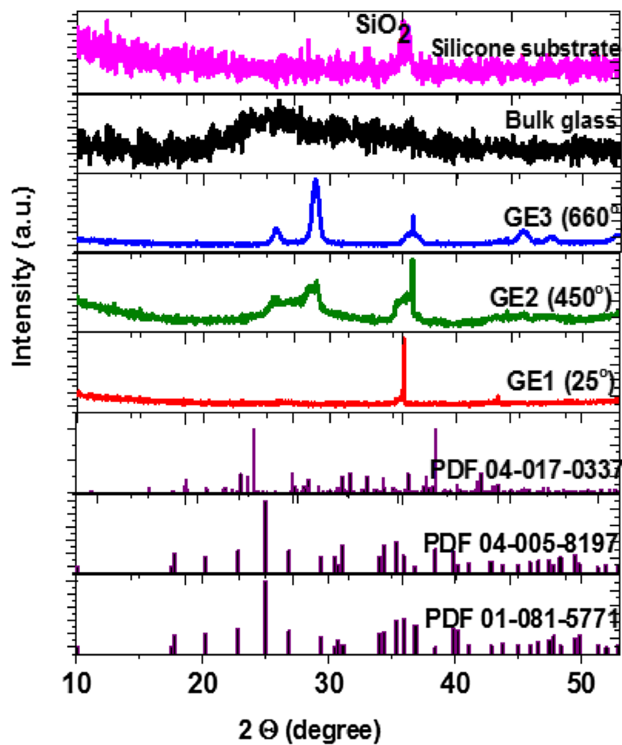

Fig. 3 XRD patterns for a pure silicon substrate (thickness = 675 μm), Er^{3+}-doped Ga–La–S bulk glass, and thin films deposited on silicon at various substrate temperature

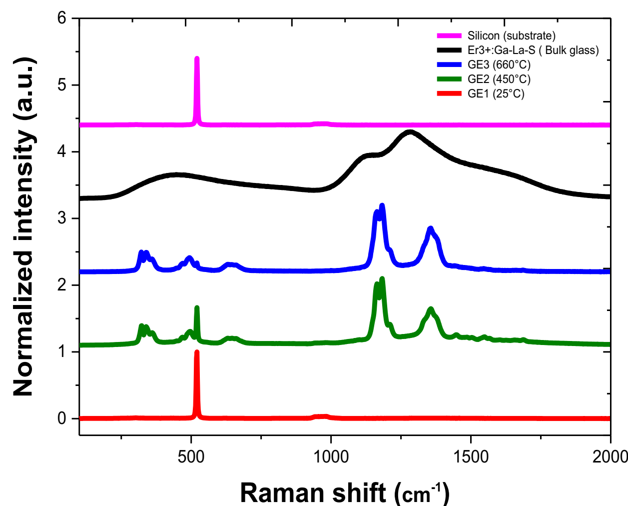

Fig. 4 Raman spectra of a pure silicon substrate (thickness = 675 μm), Er^{3+}-doped Ga–La–S bulk glass, and thin films on silicon at various substrate temperatures

stretching vibrations, which is consistent with Lucazeau et al. [35]. However, the clearly split strong Raman bands peaking at 1200 cm^{-1} and 1350 cm^{-1} exhibit the characteristic features of Er^{3+}-doped crystalline thin films, due to the Er^{3+} ions PL under 514.5 nm laser excitation [33].

3.2 Optical properties of Er^{3+}-doped Ga–La–S thin films

The PL spectra of Er^{3+}-doped Ga–La–S target glass and thin films are recorded at room temperature using a 980 nm excitation source and illustrated in Fig. 5a. The PL spectra peak around 1.54 μm corresponded to the $^4I_{13/2}$–$^4I_{15/2}$ transition of the Er^{3+} ions and the energy diagram is depicted in Fig. 5b. Figure 5a shows a very intense peak for all samples with spectral full width at half maximum (FWHM) ~ 50 nm, while the target chalcogenide glass exhibits a much broader FWHM of ~ 75 nm. Also, sample GE3 exhibits five multiples sharp peaks known as Stark levels, which can be attributed to the thermal population of the higher levels of the 1.54 μm manifold. The presence of these transitions from Stark levels clearly confirms the crystalline phases of the doped material present in the thin film.

Table 1 shows the PL lifetime (τ_f) measurement data for Er^{3+}-doped Ga–La–S target glass and various thin films. The results obtained are summarised in Table 1. The lifetime of the $^4I_{13/2}$ transition for the thin films decrease very rapidly from 1.82 to 0.46 ms with increasing deposition temperature, which confirms the changes in the local crystal field. The drop in measured fluorescence lifetime of thin film prepared at room temperature to that corresponding to the bulk glass is attributed to reabsorption that results in longer measured lifetimes in bulk glasses [36–38]. In powders and thin films of Er^{3+}-doped chalcogenide glasses, the measured lifetimes are more accurate and comparable to radiative lifetimes [34]. Another attribute to the drop in lifetime is the higher presence of –OH radicals in thin film compared to bulk glasses that result in nonradioactive relaxation of the $^4I_{13/2}$ level, leading to a reduction in the measured lifetime. In our studies, as the deposition temperature increased, we also observed that the crystallinity of the films increased as reported in the XRD of Fig. 3. This results in more Er^{3+}-ions being incorporated into the crystalline phases reported above, leading to Er^{3+} ion–ion interactions and self-quenching of photoluminescence and subsequently lower measured lifetime [39, 40]. The drop in measured lifetime with film preparation temperature can be understood on this basis.

The transmission spectra of the thin films are measured using the UV–Vis–NIR spectrometer in the wavelength range between 320 and 2000 nm. Thus, the absorption coefficient (α) spectra are determined from transmission through the thin films by the approximate expression [41, 42].

$$T = (1 - R)^2 e^{-\alpha d}, \tag{2}$$

where T is the transmission, R is the reflectance, and d is the thickness of the film, assuming that the reflectance of these thin films is very low in the photon energy range of interest.

The optical band gap energy of Er-doped Ga–La–S glass thin films prepared is calculated from the UV–Vis absorption edge by using the absorption coefficient obtained from

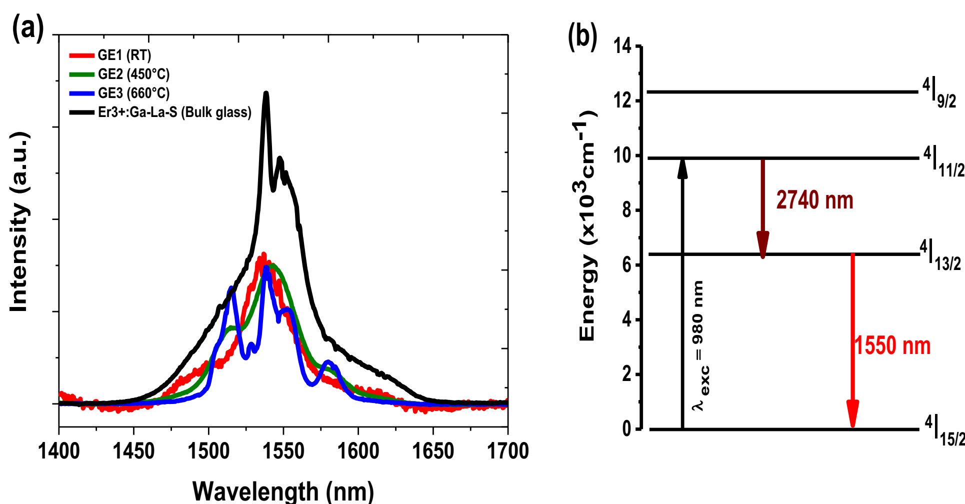

Fig. 5 **a** Photoluminescence (PL) spectra of 1 mol% Er^{3+}-doped Ga–La–S glass and Er^{3+}-doped Ga–La–S thin films deposited at various substrate temperatures. **b** Energy transfer sketch of Er^{3+}-doped glass when pumped at 980 nm

Table 1 Fluorescence lifetimes of Er^{3+}-doped Ga–La–S samples at different substrate temperatures

Er^{3+}-doped Ga–La–S samples	Fluorescence lifetime τ (ms)
Bulk glass	4.87
GE1 (25 °C)	1.82
GE2 (450 °C)	0.59
GE3 (660 °C)	0.46

transmission measurements and Tauc optical band gap relation [43, 44]:

$$\alpha h\nu = B(h\nu - E_g)^n, \quad (3)$$

where α is the absorption coefficient, $h\nu$ is the energy of incident photons, E_g is the optical band gap, B is the band tailing forbidden. n symbolises the transition process which could take values 1/2, 1, 3/2, or 2 for direct allowed, indirect allowed, direct forbidden, and indirect forbidden transitions depending on the electronic transitions responsible for the absorption.

The optical band gap is calculated by using $n = 1/2$ for direct allowed from the absorption spectra, which exhibits a perfect fit for all the thin film samples. Figure 6a shows the plots of $(\alpha h\upsilon)^2$ as a function of $h\upsilon$ (eV). Sample GE1 prepared at low temperature has a strong absorption with E_g around ~2.15 eV, and then decreases gradually with increase in deposition temperature to E_g values of 1.90 eV and 1.75 eV for sample GE2 and GE3 thin films, as depicted in Fig. 6b. As discussed before, when the temperature of the film increased from room temperature to 660 °C, the films were found to be more crystalline. This is confirmed by the average crystallite size estimated from the XRD data for samples GE2 and GE3. Henceforth, the change in optical band gap is inversely dependent on the diameter of the crystalline size [32, 45, 46], which explains the decrease in the observed band gap E_g with increase in deposition temperature [46, 47]. Similar results have been reported previously for optical absorption of

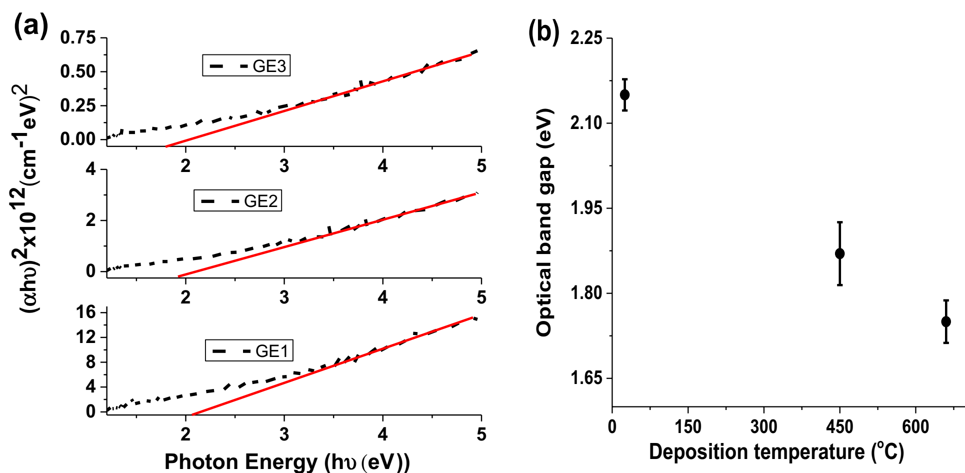

Fig. 6 **a** Tauc plot as a function of photon energy and **b** optical band gap versus deposition temperature of Er^{3+}-doped Ga–La–S glass thin films on a silicon substrate

Ga–La–S thin film [12] samples fabricated by employing different deposited energy densities.

4 Conclusions

In summary, Er^{3+}-doped Ga–La–S glass thin films were successfully deposited on the pure silicon substrate at various temperatures by using the fs-PLD technique. The effect of deposition temperature on the thickness and crystalline structure of the deposited films has been systematically investigated, which clearly show that an increase in deposition temperature corresponds to increase in film thickness and crystalline phases. The structural characteristics of the target chalcogenide glass changes from amorphous to crystalline phase as well. However, no intermixing and interdiffusion behaviour is observed between the silicon substrate and the deposited layer, which could link to the quality of the chalcogenide target glass, since fs-PLD-assisted induced intermixing is actually dependent on the target and substrate materials. The PL spectra of as-deposited Er^{3+}-doped Ga–La–S chalcogenide thin films at various temperatures exhibit very intense emission signal at 1534 nm under a pump wavelength of 980 nm with FWHM at ~ 50 nm. On the other hand, the PL lifetime at $^4I_{13/2}$ transition decreases with increase in deposition temperature as discussed; clear temperature dependences of the lifetime could be associated with increasing Er^{3+} ion concentration in the thin films and non-radiative decay or change in the local crystal field. Finally, a large optical band gap was observed from the film prepared at the low deposition temperature. The decrease in band gap with the increase in deposition temperature is associated with increase in film thickness, as well as structural modification of the thin films. The structural and optical properties of these films show their promising use in devices such as lasers and optical amplifiers opportunities.

Acknowledgements The authors from the University of Leeds appreciate the Engineering and Physical Science Research Council (EPSRC) financial support through the SeaMatics research Grant (EP/M015165/1). The authors acknowledge the financial support from the Saudi Ministry of Education and Umm al-Qura University (PhD scholarship for Kheir Saad Albarkaty). The University of Southampton acknowledges the support of the EPSRC through Grant EP/M015130/1 Manufacturing and Application of Next Generation Chalcogenides. There is no underpinning data which requires archiving and reasonable requests for data will be met where possible.

Open Access This article is distributed under the terms of the Creative Commons Attribution 4.0 International License (http://creativecommons.org/licenses/by/4.0/), which permits unrestricted use, distribution, and reproduction in any medium, provided you give appropriate credit to the original author(s) and the source, provide a link to the Creative Commons license, and indicate if changes were made.

References

1. A. Zakery, S.R. Elliott, *Optical Nonlinearities in Chalcogenide Glasses and their Applications* (Springer, Berlin, 2007)
2. A. B. Seddon, J. Non-Cryst. Solids **184**, 44 (1995)
3. V.G. Ta'eed, N.J. Baker, L. Fu, K. Finsterbusch, M.R.E. Lamont, D.J. Moss, H.C. Nguyen, B.J. Eggleton, D.Y. Choi, S. Madden, B. Luther-Davies, Opt. Express, **15**(15), 9205 (2007)
4. R.C. Schimmel, A.J. faber, H. de Waardt, G.D. Khoe, J. Non-Cryst. Solids **284**, 188 (2001)
5. A.K. Mairaj, R.J. Curry, D.W. Hewak, Electron. Lett. **40**(7), 1 (2004)
6. K. Mairaj, M.N. Petrovich, Y.W. West, A. Fu, D.W.J. Harwood, L.N. Ng, T.M. Monro, N.G. Broderick, D.W. Hewak, SPIE Fiber Opt. Sens. Technol. II Part **B4204**, 278 (2001)
7. M.S.B. Darby, R.E. Simpson, T.C. May-Smith, D.W. Hewak, R.W. Eason, J. Non-Cryst. Solids **354**, 4582 (2008)
8. P. Bastock, C. Craig, K. Khan, E. Weatherby, J. Yao, D.W. Hewak, Properties of gallium lanthanum sulphide glass, lasers and electro-optics (CLEO, 1, 2015 conference on, IEEE Xplore), pp 2160–8989
9. D.S. Gill, R.W. Eason, C. Zaldo, H.N. Rutt, N.A. Vainos, J. Non-Cryst. Solids **191**, 321 (1995)
10. V. Pruneri, P.G. Kazansky, D. Hewak, J. Wang, H. Takebe, D.N. Payne, Appl. Phys. Lett. **70**, 155 (1997)
11. M.T. de Araujo, J.A. Medeiros Neto, A.S.B. Sombra, A.S. Oliveira, A.S. Gouveia-Neto, Opt. Mater. **7**, 1 (1997)
12. R. Asal, H.N. Rutt, Opt. Mater. **8**(4), 259 (1997)
13. C. C. Ye, D.W. Hewak, M. Hempstead, B.N. Samson, D.N. Payne, J. Non-Cryst. Solids **208**, 56 (1996)
14. J.A. Frantz, J.S. Sanghera, L.B. Shaw, G. Villalobos, I.D. Aggarwal, D.W. Hewak, Mater. Lett. **60**, 1350 (2006)
15. T. Schweizer, D.W. Hewak, D. Payne, T. Jensen, G. Huber, Neodymium-doped gallium lanthanum sulphide glass laser, in *At Conference on Lasers and Electro-Optics (CLEO Europe) Conference on Lasers and Electro-Optics (CLEO Europe), CFD3*, 08–13 Sep (1996), Germany
16. C. C. Huang, D.W. Hewak, Electron. Lett. **40**, 863 (2004)
17. M. Churbanov, I. Scripachev, V. Shiryaev, V. Plotnichenko, S. Smetanin, E. Kryukova, Y.N. Pyrkov, B. Galagan, J. Non-Cryst. Solids **326**, 301 (2003)
18. S. Song, N. Carlie, J. Boudies, L. Petit, K. Richardson, C.B. Arnold, J. Non-Cryst. Solids **355**, 2272 (2009)
19. C. C. Huang, D.W. Hewak, J.V. Badding, Opt. Express **12**(11), 2501 (2004)
20. N. Anscombe, D.W. Hewak, Nat. Photon. **5**(8), 474 (2011)
21. D. A. Turnbull, S.J. Sanghera, V. Nguyen, I.D. Aggarwal, Mater. Lett. **58**, 51 (2004)
22. M. Frumar, B. Frumarova, P. Nemec, T. Wagner, J. Jedelsky, M. Hrdlicka, J. Non-Cryst. Solids **352**, 544 (2006)
23. K.E. Youden, T. Grevatt, R.W. Eason, H.N. Rutt, R.S. Deol, G. Wylangowski, Appl. Phys. Lett. **63**, 1601 (1993)
24. A. Zakery, Y. Ruan, A.V. Rode, M. Samoc, B. Luther-Davies, J. Opt. Soc. Am. B **20**, 1844 (2003)
25. V. Nazabal, P. Němec, J. Jedelsky, C. Duverger, J. Le Person, J.L. Adam, M. Frumar, Opt. Mater. **29**, 273 (2006)
26. P. Němec, V. Nazabal, M. Pavlista, A. Moreac, M. Frumar, M. Vlcek, Mater. Chem. Phys. **117**, 23 (2009)
27. T. Teghil, L.D. Alessio, A. Santagata, M. Zaccagnino, D. Ferro, D.J. Sordelet, Appl. Surf. Sci. **210**, 307 (2003)
28. C. Momma, B.N. Chichkov, S. Nolte, F. von Alvensleben, A. Tünnermann, H. Welling, B. Wellegehausen, Opt. Commun. **129**, 134 (1996)
29. D. Pietroy, Y. Di Maio, B. Moine, E. Audouard, Opt. Express **20**(28), 29900 (2012)

30. A. Semerok, B. Salle, J.–F. Wagner, G. Petite, Laser Part. Beams **20**, 67 (2002)
31. F. Garrelie, C. Donnett, A.S., Loir, N. Benchikh, Proc. SPIE **6261**, 62610L (2006)
32. F.G. Hone, F.K. Ampong, Mater. Chem. Phys. **183**, 320 (2016)
33. E. Kumi-Barimah, M. W. Ziarko, N. Bamiedakis, I. H. White, R. V. Penty, G. Jose, Opt. Mater. Express **8**(7), 1997 (2018)
34. Y. Jinqiu, C. Lei, H. Huaqiang, Y. Shihong, H. Yunsheng, W. Hao, J. Rare Erath's **32**(1), 1 (2014)
35. G. Lucazeau, S. Barnier, A.M. Loireau-Lozac'h. Spectrochem. Acta **34A**, 21 (1978)
36. A. Ravagli, N.G. Boetti, F.A. Guzman Cruz, G.A. Alzaidy, D. Pugliese, D. Milanese, D.W. Hewak, R. Soc. Chem. Adv. **8**, 27556 (2018)
37. C. Kouhia, C. Craig, D.W. Hewak, S. Kasap, Opt. Mater. **41**, 116 (2015)
38. C. Kouhia, S.O. Kasap, Opt. Express **16**, 1343 (2008)
39. A. J. Faber, D.R. Simons, Y. Yan, H. de Waal, Proc. SPIE **2290**, 80 (1994)
40. R. Morea, J. Fernandez, R. Balda, J. Gonzalo, Proc. SPIE **9744**, 974402–974401 (2017)
41. T. Guang-Lei, H. Hong-Bo, S. Jian-Da, Chin. Phys. Lett. **22**, 1787 (2005)
42. S. Baco, A. Chik, F.M. Yassin, J. Sci. Technol. **4**, 61 (1999)
43. T.M. Mok, S.K. O'Leary, J. Appl. Phys. **102**, 113525 (2007)
44. O.G. Pompilian, G. Dascalu, I. Mihaila, S. Gurlui, M. Olivier, P. Nemec, V. Nazabal, N. Cimpoesu, C. Focsa, Appl. Phys. A **117**, 197 (2014)
45. M. El-Zahed, M. Dongol, Radwan, Eur. Phys. J. Appl. Phys. **17**, 179–186 (2002)
46. A. El-korashy, M. A. Abdel-Rahim, H. El-Zahed, Thin Solid Films **338**, 207–213 (1999)
47. H. El-Zahed, M. Dongol, M. Radwan, Eur. Phys. J. Appl. Phys. **17**, 179 (2002)